Non-unique Games over Compact Groups and Orientation Estimation in Cryo-EM

Amit Singer

Princeton University

Department of Mathematics and Program in Applied and Computational Mathematics

July 28, 2016

NIH National Institute of General Medical Sciences
Basic Discoveries for Better Health

GORDON AND BETTY MOORE FOUNDATION

SIMONS FOUNDATION

AIR FORCE OFFICE OF SCIENTIFIC RESEARCH
UNITED STATES AIR FORCE

Single Particle Reconstruction using cryo-EM

Schematic drawing of the imaging process:

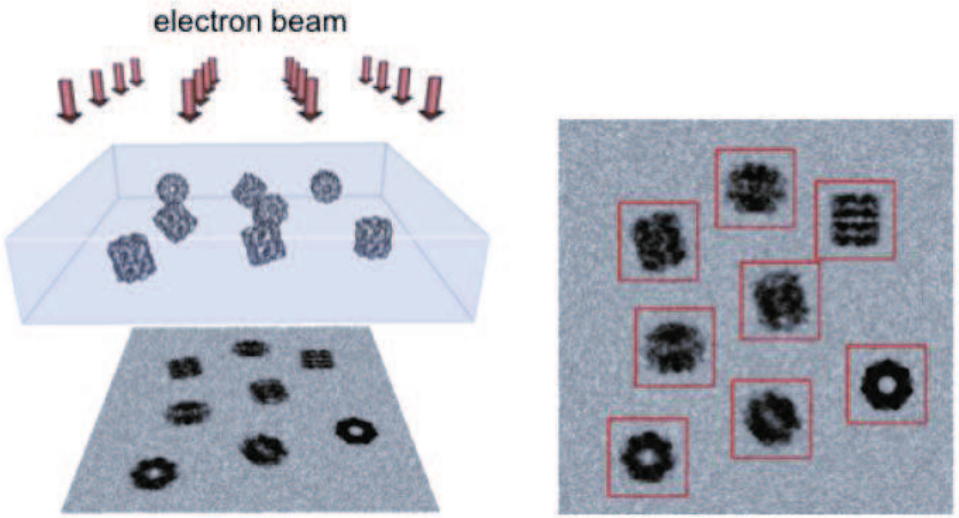

The cryo-EM problem:

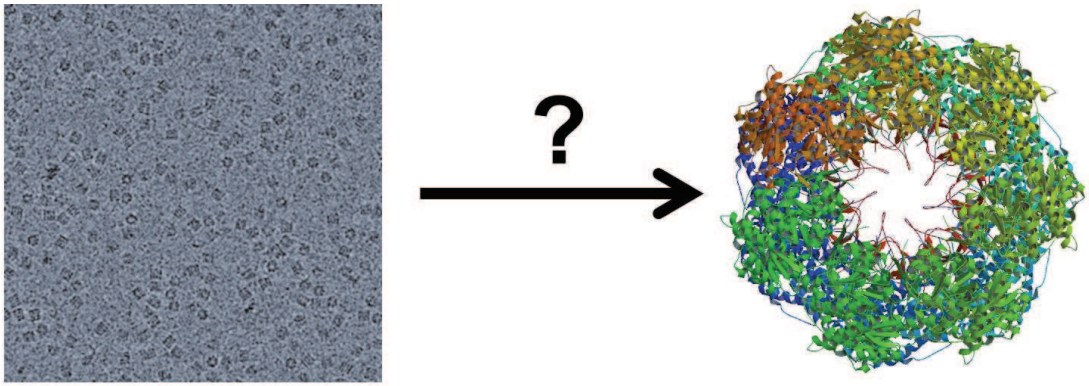

tomographic image

3-D structure

www.sciencemag.org **SCIENCE** VOL 343 28 MARCH 2014

BIOCHEMISTRY

The Resolution Revolution

Advances in detector technology and image processing are yielding high-resolution electron cryo-microscopy structures of biomolecules.

Werner Kühlbrandt

Precise knowledge of the structure of macromolecules in the cell is essential for understanding how they function. Structures of large macromolecules can now be obtained at near-atomic resolution by averaging thousands of electron microscope images recorded before radiation damage accumulates. This is what Amunts *et al*. have done in their research article on page 1485 of this issue (*1*), reporting the structure of the large subunit of the mitochondrial ribosome at 3.2 Å resolution by electron cryo-microscopy (cryo-EM). Together with other recent high-resolution cryo-EM structures (*2*–*4*) (see the figure), this achievement heralds the beginning of a new era in molecular biology, where structures at near-atomic resolution are no longer the prerogative of x-ray crystallography or nuclear magnetic resonance (NMR) spectroscopy.

Ribosomes are ancient, massive protein-RNA complexes that translate the linear genetic code into three-dimensional proteins.

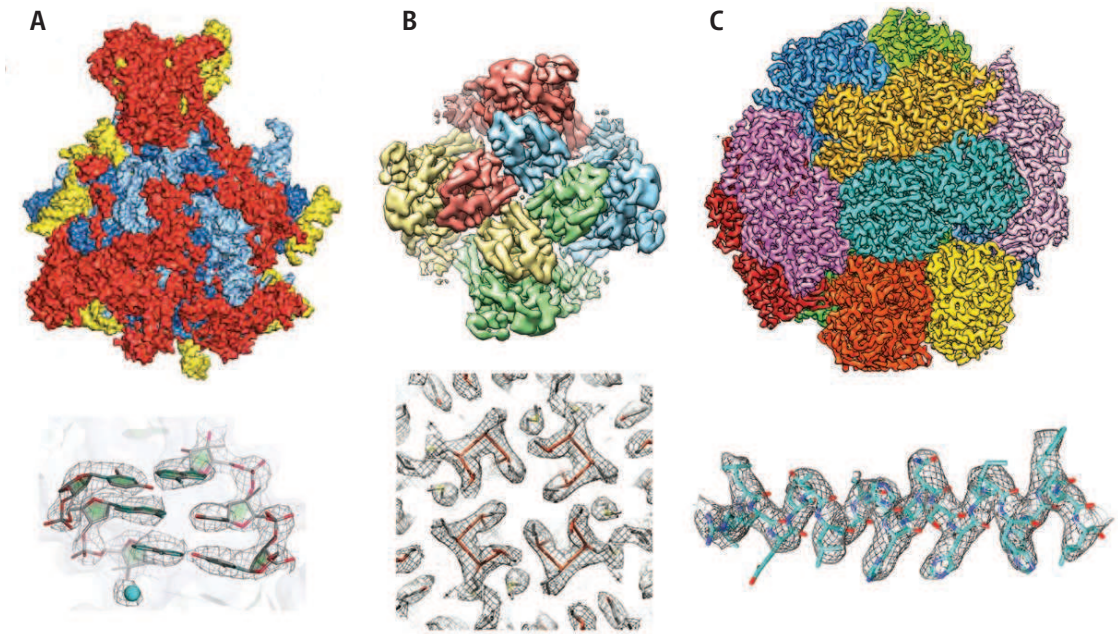

Near-atomic resolution with cryo-EM. (**A**) The large subunit of the yeast mitochondrial ribosome at 3.2 Å reported by Amunts *et al*. In the detailed view below, the base pairs of an RNA double helix and a magnesium ion (blue) are clearly resolved. (**B**) TRPV1 ion channel at 3.4 Å (*2*), with a detailed view of residues lining the ion pore on the four-fold axis of the tetrameric channel. (**C**) F_{420}-reducing [NiFe] hydrogenase at 3.36 Å (*3*). The detail shows an α helix in the FrhA subunit with resolved side chains. The maps are not drawn to scale.

Cryo-EM in the news...

March 31, 2016

Science

REPORTS

Cite as: Sirohi *et al.*, *Science* 10.1126/science.aaf5316 (2016).

The 3.8 Å resolution cryo-EM structure of Zika virus

Devika Sirohi,[1]* Zhenguo Chen,[1]* Lei Sun,[1] Thomas Klose,[1] Theodore C. Pierson,[2] Michael G. Rossmann,[1]† Richard J. Kuhn[1]†

[1]Markey Center for Structural Biology and Purdue Institute for Inflammation, Immunology and Infectious Disease, Purdue University, West Lafayette, IN 47907, USA. [2]Viral Pathogenesis Section, Laboratory of Viral Diseases, National Institute of Allergy and Infectious Diseases, National Institutes of Health, Bethesda, MD 20892, USA.

Method of the Year 2015

January 2016 Volume 13 No 1

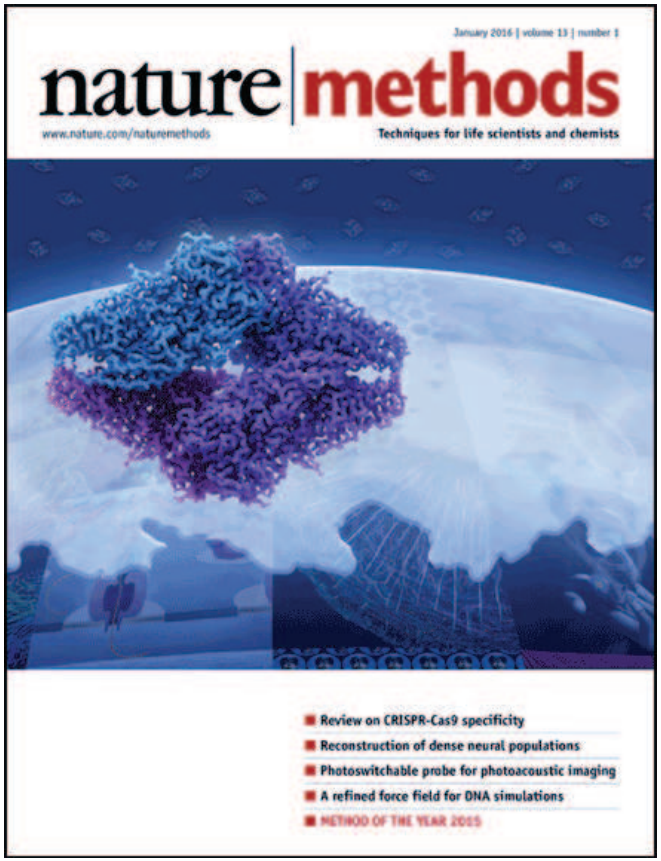

Single-particle cryo-electron microscopy (cryo-EM) is our choice for Method of the Year 2015 for its newfound ability to solve protein structures at near-atomic resolution. Featured is the 2.2-Å cryo-EM structure of β-galactosidase as recently reported by Bartesaghi *et al.* (***Science* 348, 1147–1151, 2015**). Cover design by Erin Dewalt.

Big "Movie" Data, Publicly Available

http://www.ebi.ac.uk/pdbe/emdb/empiar/

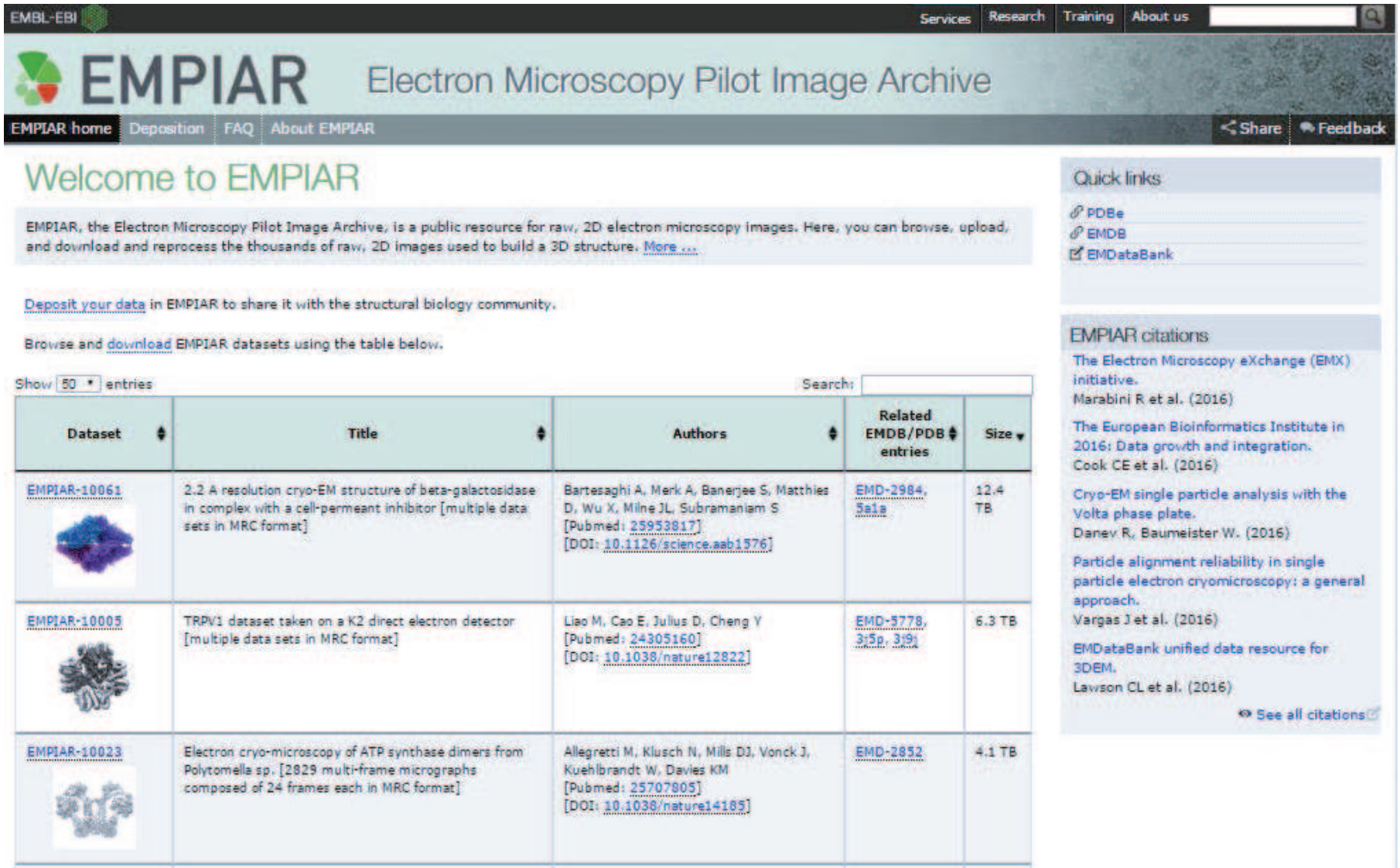

EMBL-EBI

Services | Research | Training | About us

EMPIAR Electron Microscopy Pilot Image Archive

EMPIAR home | Deposition | FAQ | About EMPIAR | Share | Feedback

Welcome to EMPIAR

EMPIAR, the Electron Microscopy Pilot Image Archive, is a public resource for raw, 2D electron microscopy images. Here, you can browse, upload, and download and reprocess the thousands of raw, 2D images used to build a 3D structure. More ...

Deposit your data in EMPIAR to share it with the structural biology community.

Browse and download EMPIAR datasets using the table below.

Show 50 entries Search:

Dataset	Title	Authors	Related EMDB/PDB entries	Size
EMPIAR-10061	2.2 A resolution cryo-EM structure of beta-galactosidase in complex with a cell-permeant inhibitor [multiple data sets in MRC format]	Bartesaghi A, Merk A, Banerjee S, Matthies D, Wu X, Milne JL, Subramaniam S [Pubmed: 25953817] [DOI: 10.1126/science.aab1576]	EMD-2984, 5a1a	12.4 TB
EMPIAR-10005	TRPV1 dataset taken on a K2 direct electron detector [multiple data sets in MRC format]	Liao M, Cao E, Julius D, Cheng Y [Pubmed: 24305160] [DOI: 10.1038/nature12822]	EMD-5778, 3j5p, 3j9i	6.3 TB
EMPIAR-10023	Electron cryo-microscopy of ATP synthase dimers from Polytomella sp. [2829 multi-frame micrographs composed of 24 frames each in MRC format]	Allegretti M, Klusch N, Mills DJ, Vonck J, Kuehlbrandt W, Davies KM [Pubmed: 25707805] [DOI: 10.1038/nature14185]	EMD-2852	4.1 TB

Quick links

- PDBe
- EMDB
- EMDataBank

EMPIAR citations

The Electron Microscopy eXchange (EMX) initiative.
Marabini R et al. (2016)

The European Bioinformatics Institute in 2016: Data growth and integration.
Cook CE et al. (2016)

Cryo-EM single particle analysis with the Volta phase plate.
Danev R, Baumeister W. (2016)

Particle alignment reliability in single particle electron cryomicroscopy: a general approach.
Vargas J et al. (2016)

EMDataBank unified data resource for 3DEM.
Lawson CL et al. (2016)

See all citations

E. coli 50S ribosomal subunit

27,000 particle images provided by Dr. Fred Sigworth, Yale Medical School

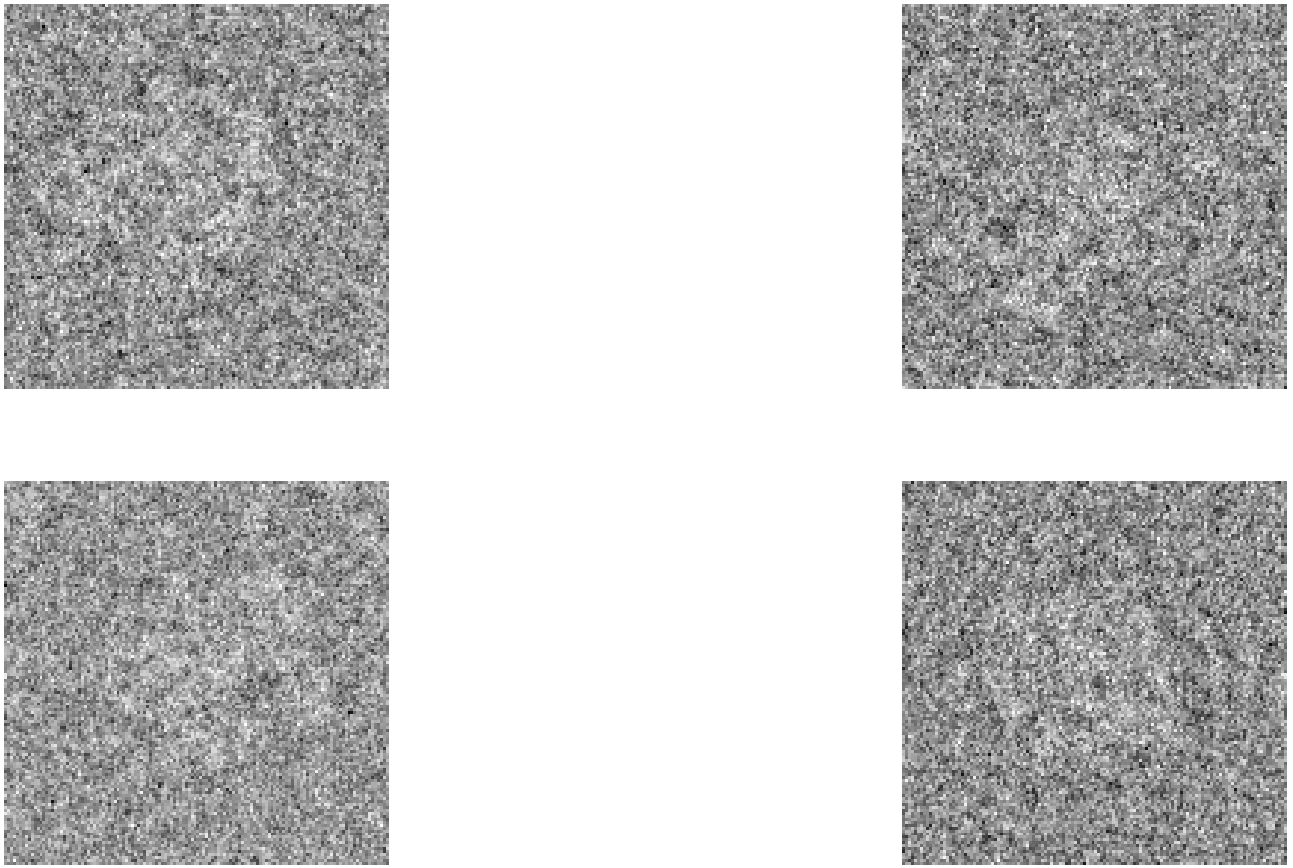

3D reconstruction by S, Lanhui Wang, and Jane Zhao

Orientation Estimation: Fourier projection-slice theorem

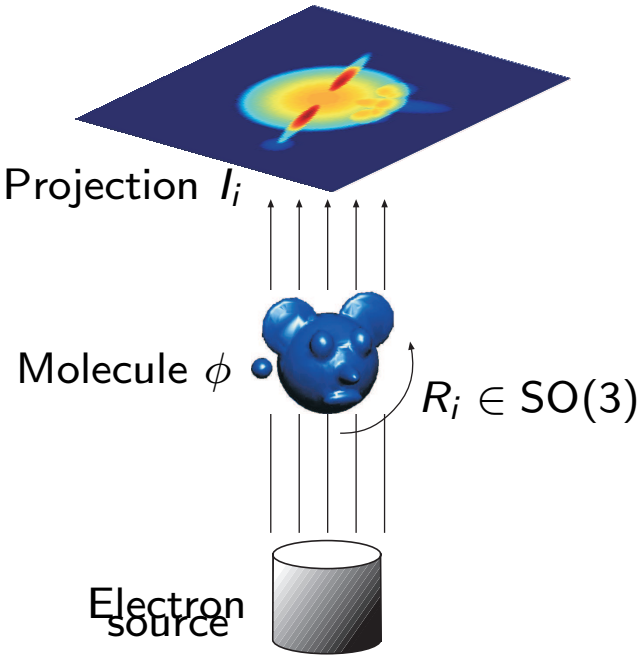

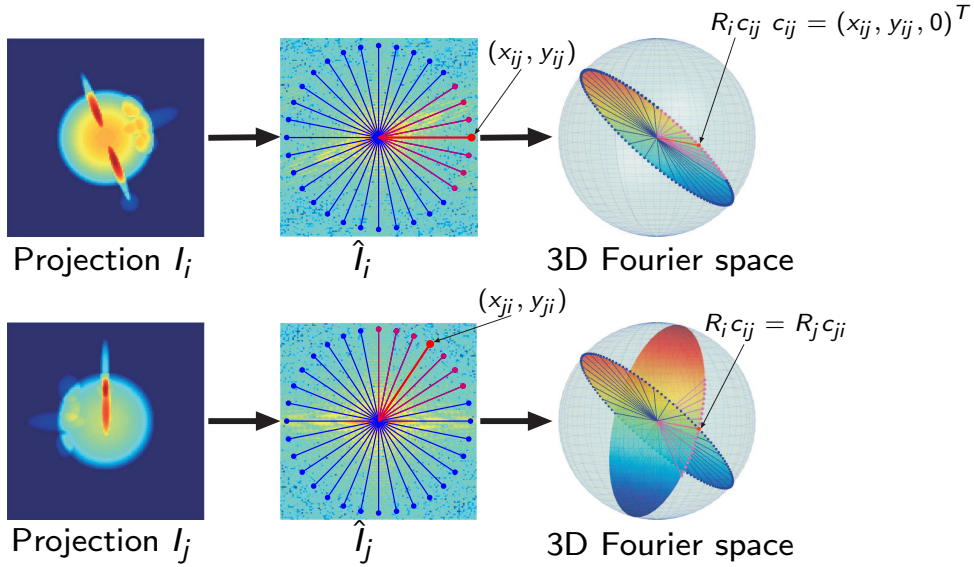

- Cryo-EM inverse problem: Find ϕ (and $R_1, \ldots, R_n$) given $I_1, \ldots, I_n$.
- $n = 3$: Vainshtein and Goncharov 1986, van Heel 1987
- $n > 3$: S, Shkolnisky (SIAM Imaging 2011)

$$\min_{R_1, R_2, \ldots, R_n \in SO(3)} \sum_{i \neq j} \| R_i c_{ij} - R_j c_{ji} \|^2$$

Maximum Likelihood Estimation

- The images contain more information than that expressed by optimal pairwise matching of common lines.
- Algorithms based on pairwise matching can succeed only at "high" SNR.
- We would like to try all possible rotations $R_1, \ldots, R_n$ and choose the combination for which the agreement on the common lines (implied by the rotations) as observed in the images is maximal.
- Computationally intractable: exponentially large search space, complicated cost function.

$$\min_{g_1,\ldots,g_n \in G} \sum_{i,j=1}^{n} f_{ij}(g_i g_j^{-1})$$

3D Puzzle

$G = SO(3)$

$$\min_{g_1,g_2,\ldots,g_n \in G} \sum_{i,j=1}^{n} f_{ij}(g_i g_j^{-1})$$

Non-Unique Games over Compact Groups

- Optimization problem:

$$\min_{g_1,g_2,\ldots,g_n \in G} \sum_{i,j=1}^{n} f_{ij}(g_i g_j^{-1})$$

  G is a compact group, $f_{ij} : G \to \mathbb{R}$ smooth, bandlimited functions.
- Parameter space $G \times G \times \cdots \times G$ is exponentially large.
- For $G = \mathbb{Z}_2 = \{-1, +1\}$ this encodes Max-Cut, which is NP-hard.

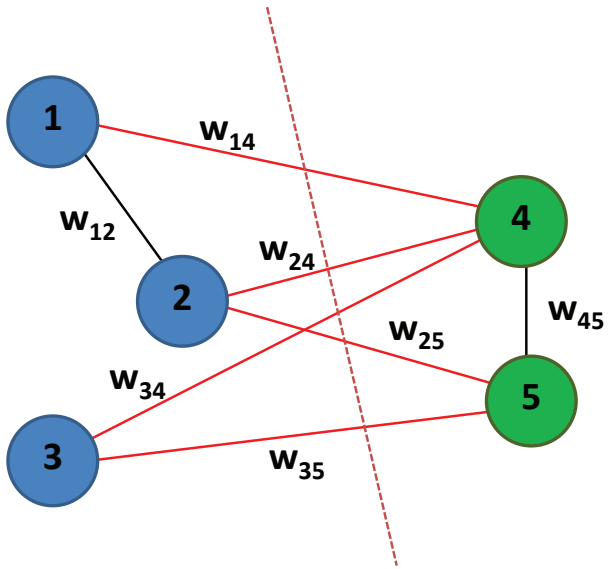

Why non-unique games?

- Max-2-Lin($\mathbb{Z}_L$) formulation of Unique Games (Khot et al 2005): Find $x_1, \ldots, x_n \in \mathbb{Z}_L$ that satisfy as many difference eqs as possible

$$x_i - x_j = b_{ij} \mod L, \quad (i,j) \in E$$

- This corresponds to $G = \mathbb{Z}_L$ and

$$f_{ij}(x) = \begin{cases} -1 & x = b_{ij} \\ 0 & x \neq b_{ij} \end{cases}$$

in

$$\min_{x_1, x_2, \ldots, x_n \in \mathbb{Z}_L} \sum_{i,j=1}^{n} f_{ij}(x_i - x_j)$$

- Our games are non-unique in general, and the group is not necessarily finite.

Fourier transform over G

- Recall for $G = SO(2)$

$$f(\alpha) = \sum_{k=-\infty}^{\infty} \hat{f}(k) e^{\imath k \alpha}$$

$$\hat{f}(k) = \frac{1}{2\pi} \int_0^{2\pi} f(\alpha) e^{-\imath k \alpha} \, d\alpha$$

- In general, for a compact group G

$$f(g) = \sum_{k=0}^{\infty} d_k \mathrm{Tr}\left[\hat{f}(k) \rho_k(g)\right]$$

$$\hat{f}(k) = \int_G f(g) \rho_k(g)^* \, dg$$

- Here
  - ρ_k are the unitary irreducible representations of G
  - d_k is the dimension of the representation ρ_k (e.g., $d_k = 1$ for $SO(2)$, $d_k = 2k+1$ for $SO(3)$)
  - dg is the Haar measure on G

Linearization of the cost function

- Introduce matrix variables ("matrix lifting")

$$X_{ij}^{(k)} = \rho_k(g_i g_j^{-1})$$

- Fourier expansion of f_{ij}

$$f_{ij}(g) = \sum_{k=0}^{\infty} d_k \mathrm{Tr}\left[\hat{f}_{ij}(k)\rho_k(g)\right]$$

- Linear cost function

$$f(g_1, \ldots, g_n) = \sum_{i,j=1}^{n} f_{ij}(g_i g_j^{-1}) = \sum_{i,j=1}^{n}\sum_{k=0}^{\infty} d_k \mathrm{Tr}\left[\hat{f}_{ij}(k) X_{ij}^{(k)}\right]$$

Constraints on the variables $X_{ij}^{(k)} = \rho_k(g_i g_j^{-1})$

1. $X^{(k)} \succeq 0$
2. $X_{ii}^{(k)} = I_{d_k}$, for $i = 1, \ldots, n$
3. $\mathrm{rank}(X^{(k)}) = d_k$

$$X_{ij}^{(k)} = \rho_k(g_i g_j^{-1}) = \rho_k(g_i)\rho_k(g_j^{-1}) = \rho_k(g_i)\rho_k(g_j)^*$$

$$X^{(k)} = \begin{bmatrix} \rho_k(g_1) \\ \rho_k(g_2) \\ \vdots \\ \rho_k(g_n) \end{bmatrix} \begin{bmatrix} \rho_k(g_1)^* & \rho_k(g_2)^* & \cdots & \rho_k(g_n)^* \end{bmatrix}$$

- We drop the non-convex rank constraint.
- The relaxation is too loose, as we can have $X_{ij}^{(k)} = 0$ (for $i \neq j$).
- Even with the rank constraint, nothing ensures that $X_{ij}^{(k)}$ and $X_{ij}^{(k')}$ correspond to the same group element $g_i g_j^{-1}$.

Additional constraints on $X_{ij}^{(k)} = \rho_k(g_i g_j^{-1})$

- The delta function for $G = SO(2)$

$$\delta(\alpha) = \sum_{k=-\infty}^{\infty} e^{\imath k \alpha}$$

- Shifting the delta function to $\alpha_i - \alpha_j$

$$\delta(\alpha - (\alpha_i - \alpha_j)) = \sum_{k=-\infty}^{\infty} e^{\imath k \alpha} e^{-\imath k(\alpha_i - \alpha_j)} = \sum_{k=-\infty}^{\infty} e^{\imath k \alpha} X_{ij}^{(k)^*}$$

- The delta function is non-negative and integrates to 1:

$$\sum_{k=-\infty}^{\infty} e^{\imath k \alpha} X_{ij}^{(k)^*} \geq 0, \quad \forall \alpha \in [0, 2\pi)$$

$$\frac{1}{2\pi} \int_0^{2\pi} \sum_{k=-\infty}^{\infty} e^{\imath k \alpha} X_{ij}^{(k)^*} \, d\alpha = X_{ij}^{(0)^*} = 1$$

Finite truncation via Fejér kernel

- In practice, we cannot use infinite number of representations to compose the delta function.
- Simple truncation leads to the Dirichlet kernel which changes sign

$$D_m(\alpha) = \sum_{k=-m}^{m} e^{\imath k\alpha}$$

- This is also the source for the Gibbs phenomenon and the non-uniform convergence of the Fourier series.
- The Fejér kernel is non-negative

$$F_m(\alpha) = \frac{1}{m}\sum_{k=0}^{m-1} D_k(\alpha) = \sum_{k=-m}^{m}\left(1 - \frac{|k|}{m}\right) e^{\imath k\alpha}$$

- The Fejér kernel is the first order Cesàro mean of the Dirichlet kernel.

Finite truncation via Fejér-Riesz factorization

- Non-negativity constraints over $SO(2)$

$$\sum_{k=-m}^{m} \left(1 - \frac{|k|}{m}\right) e^{\imath k\alpha} X_{ij}^{(k)^*} \geq 0, \quad \forall \alpha \in [0, 2\pi)$$

- Fejér-Riesz: P is a non-negative trigonometric polynomial over the circle, i.e. $P(e^{\imath\alpha}) \geq 0 \ \forall \alpha \in [0, 2\pi)$ iff $P(e^{\imath\alpha}) = |Q(e^{\imath\alpha})|^2$ for some polynomial Q.
- Leads to semidefinite constraints on $\left\{X_{ij}^{(k)}\right\}_k$ for each i, j.
- Similar non-negativity constraints hold for general G using the delta function over G

$$\delta(g) = \sum_{k=0}^{\infty} d_k \mathrm{Tr}\left[\rho_k(g)\right]$$

- For example, Fejér proved that for $SO(3)$ the second order Cesàro mean of the Dirichlet kernel is non-negative.

Additional constraints for $SO(3)$

- $X_{ij}^{(k)}$ is a representation of $SO(3)$.
- $X_{ij}^{(0)} = 1$
- $X_{ij}^{(1)} \in \mathrm{conv} SO(3)$ is a semidefinite constraint using unit quaternions and Euler-Rodrigues formula
  (Saunderson, Parrilo, Willsky SIOPT 2015)

$$Q = qq^T : \qquad Q \succeq 0, \qquad \mathrm{Tr}(Q) = 1, \qquad Q = T(X_{ij}^{(1)})$$

- $X_{ij}^{(k)}$ sum-of-squares relaxation

Tightness of the semidefinite program

- We solve an SDP for the matrices $X^{(1)}, \ldots, X^{(m)}$.
- Numerically, the solution of the SDP has the desired ranks up to a certain level of noise (w.h.p).
- In other words, even though the search-space is exponentially large, we typically find the MLE in polynomial time.
- This is a viable alternative to heuristic methods such as EM and alternating minimization.
- The SDP gives a certificate whenever it finds the MLE.

Final Remarks

- Loss of handedness ambiguity in cryo-EM: If $g_1, \ldots, g_n \in SO(3)$ is the solution, then so is $Jg_1J^{-1}, \ldots, Jg_nJ^{-1}$ for $J = \mathrm{diag}(-1, -1, 1)$.
- Define $X_{ij}^{(k)} = \frac{1}{2}\left[\rho_k(g_i g_j^{-1}) + \rho_k(Jg_i g_j^{-1} J^{-1})\right]$
- Splits the representation: $2k+1 = d_k = k + (k+1)$, reduced computation
- Point group symmetry (cyclic, dihedral, etc.): reduces the dimension of the representation (invariant polynomials)
- Translations and rotations simultaneously: $SE(3)$ is a non-compact group, but we can map it to $SO(4)$.
- Simultaneous rotation estimation and classification

References

- A. Singer, Y. Shkolnisky, "Three-Dimensional Structure Determination from Common Lines in Cryo-EM by Eigenvectors and Semidefinite Programming", *SIAM Journal on Imaging Sciences*, **4** (2), pp. 543–572 (2011).

- A. S. Bandeira, M. Charikar, A. Singer, A. Zhu, "Multireference Alignment using Semidefinite Programming", 5th Innovations in Theoretical Computer Science (ITCS 2014).

- A. S. Bandeira, Y. Chen, A. Singer "Non-Unique Games over Compact Groups and Orientation Estimation in Cryo-EM", http://arxiv.org/abs/1505.03840.

- R. R. Lederman, A. Singer, "A Representation Theory Perspective on Simultaneous Alignment and Classification", http://arxiv.org/abs/1607.03464v1.

ASPIRE: Algorithms for Single Particle Reconstruction

Open source toolbox, publicly available:
http://spr.math.princeton.edu/